*Astronomical and Astrophysical Transactions* (*AApTr*), 2025, Vol. 35, Issue 4, pp. 483–492,
ISSN 1055-6796, Photocopying permitted by license only, ©Cambridge Scientific Publishers

# Variability properties of the blazar S5 1803+784 on the shortest timescales from July 2019 to June 2020

V.A. Guseva*, M.A. Gorbachev, M.S. Butuzova

*Crimean Astrophysical Observatory of RAS, Nauchny, Bakhchysarai District, Republic of Crimea, 298409, Russia*

*Received 15 June, 2025; accepted 2 August, 2025*

The blazar S5 1803+784 has an extensive observational time series obtained by the TESS satellite. Due to the relatively low optical brightness of the object and the large angular size of the pixel on the CCD detector, we used a relative photometry method to improve the photometric accuracy, utilizing summed data of 20–30 cuts of TESS Full Frame Images. The resulting light curves are analysed to determine the minimum characteristic variability timescale, under the condition of high statistical significance of the derived value. We then trace the evolution of short-term variability properties and their relation to photometric characteristics. The strong variation in characteristic timescales between adjacent segments of the light curve, along with the lack of correlation between variability parameters, is interpreted under the assumption that the variability arises due to changes in the Doppler factor of subcomponents within the emitting region.

*Keywords*: Blazar S5 1803+784, TESS, temporal variability characteristics, spectral variability characteristics, characteristic variability timescale

## 1 Introduction

Blazars are a subclass of active galactic nuclei (AGN) whose ultrarelativistic jets are directed at an angle less than 10° to the line of sight. The dominant portion of the radiation observed from blazars originates in these jets and is characterized by significant variability across the entire observable electromagnetic spectrum. Due to relativistic effects, the flux density of radiation produced in the jet is strongly Doppler boosted in the observer's reference frame, effectively overshadowing emission from other AGN regions. Paiano et al. (2020) reported the detection of a weak emission line identified as Mg II in S5 1803+784. The authors also note that the continuum dominates the emission. No emission lines had been detected in this source previously (Hewitt & Burbidge, 1993). The combination of these factors indicates the dominance of the continuum in the observed emission, suggesting its origin in a relativistic jet. It

*Email: Viktoriya.nikagu@gmail.com

should be noted that, according to Pushkarev et al. (2009), the estimated jet viewing angle for the blazar S5 1803+784 is 4.5°.

The study of optical emission is particularly relevant because it originates from a region near the base of the collimated jet. Variability on short timescales allows us to probe the internal structure of the jet flow (Butuzova 2021). However, optical variability on timescales ranging from fractions of a day to several days remains poorly studied due to the limitations imposed by Earth's diurnal rotation and weather conditions. Such investigations have previously been conducted through international campaigns providing quasi-continuous monitoring, the most notable being the Whole Earth Blazar Telescope (WEBT), which was applied, for example, to blazar S5 0716+714 (Bhatta et al. 2013).

A significant improvement in time series quality has become possible thanks to space missions dedicated to exoplanet searches. Although the Kepler mission had a limited field of view, its successor is the Transiting Exoplanet Survey Satellite (TESS), provides nearly full-sky coverage. TESS observes almost the entire sky by imaging regions of $24^\circ \times 96^\circ$ for 27 days per sector, with a temporal resolution ranging from 2 to 40 minutes. To analyse variability on multi-day timescales, a large volume of continuous and statistically significant data is required. This necessitates extended and quasi-regular observational series covering multiple TESS sectors. Such data series are available for targets near the ecliptic poles, where up to 13 consecutive sectors may be observed. For blazar S5 1803+784, three such series are available. In this study, we analyse the TESS observations of S5 1803+784 obtained from July 2019 to June 2020, complemented by photometric data from the Zwicky Transient Facility (ZTF) (Bellm et al. 2019). We trace the evolution of the shortest characteristic variability timescale and examine the correlation between the spectral and temporal parameters of variability.

## 2 TESS data processing

The TESS space telescope provides standard algorithms for extracting SAP and PDCSAP fluxes. As shown by the authors (Butuzova et al. 2025), these light curves cannot be applied in our case because they are strongly affected by Poisson noise. To suppress Poisson noise, the signal integration time was increased by summarizing cuts from full-frame images. The temporal resolution of the processed data was 120 min. The aperture photometry method was applied for TESS data processing (Butuzova et al. 2025). This approach allowed us to achieve a photometric accuracy better than 0.02 magnitudes. The apertures of the object and comparison stars are shown in Fig. 1. In our study, we used the aperture provided by the TESS data analysis pipeline for the blazar S5 1803+784 (Ricker et al., 2015). To estimate the background, neighboring pixels were selected for each source, since the background is irregular. The angular resolution of TESS is $21''$ per pixel.

For each summed image, we perform the following operations. From the sorted background pixel values in ascending order, the upper half, containing the high instrumental fluxes, was discarded. Then, a Wolfram Mathematica script generated 100 model background sets under the assumption of uniform distribution with the number of elements equal to the number of pixels in the aperture of the given source.

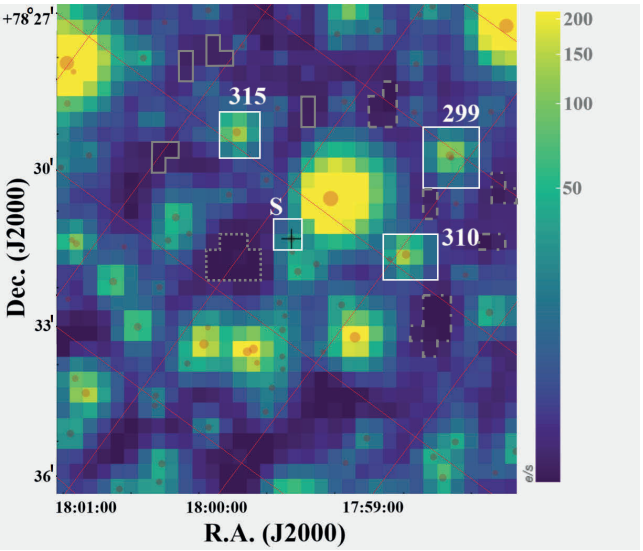



**Figure 1** Cut of a TESS full-frame image used for aperture photometry. White markers indicate the apertures, and gray regions denote the background estimation areas for the target source S5 1803+784 (S, dotted line) and the comparison stars: TIC 288432315 (315, solid line), TIC 288432299 (299, dashed line), and TIC 288432310 (310, dash-dotted line).

The total background flux from each of the 100 model sets was subtracted from the total flux of the source pixels. The instrumental flux and its uncertainty were defined as the median and standard deviation of the 100 measurements of the object's flux. The resulting accuracy for S5 1803+784 ranged from 0.5% to 1%.

## 3 Light curve and spectral index of S5 1803+784

The light curve of the blazar S5 1803+784 (see Fig. 2) was obtained using aperture photometry. Due to instrumental characteristics and the specifics of the observation method, the TESS data exhibit a nonlinear detector-dependent zero-point shift from sector to sector, which causes relative displacements between individual light curves. To mitigate this effect, we aligned the TESS data with the ZTF light curve (in the $g$ filter) by applying an additive correction of the form $1.1+k$, where $k$ is a sector-specific correction coefficient. The distribution of $k$ values follows a normal distribution with a mean of 0.03 and a standard deviation of 0.22. The corrected TESS light curves are suitable for further analysis.

The spectral index $\alpha$, defined as $F \propto \nu^{\alpha}$, was calculated using the method described by Gorbachev et al. (2024). The spectral index varied between $-1.3$ and $-1.9$ (see Fig. 3). Pearson's correlation coefficients between $\alpha$ and the magnitude were calculated for four segments that stand out visually in the top panel of Fig. 3. The maximum correlation coefficient was 0.72 and corresponded to a rapid increase in brightness along with a flattening of the spectrum during a strong flare. No overall correlation was found between the blazar's brightness and the slope of its optical

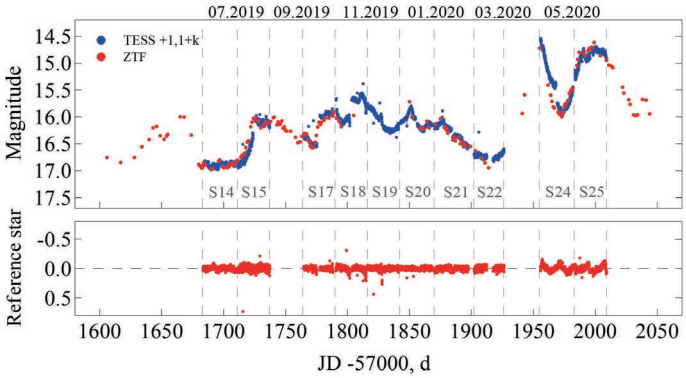



**Figure 2** Light curve of the blazar S5 1803+784 from July, 2019 to June, 2020. The labels S14 to S25 indicate the TESS sector numbers.

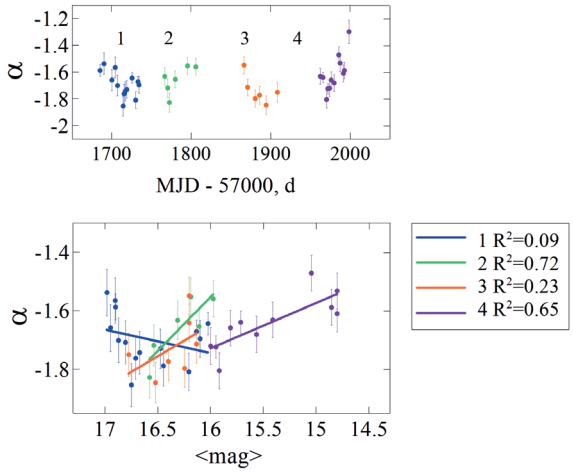



**Figure 3** The top panel shows the evolution of the spectral index of the blazar S5 1803+784 over time. The bottom right panel shows the spectral index as a function of source brightness for four distinct segments identified by eye in the top panel. The Pearson correlation coefficients are shown in the lower bottom part of the plot.

power-law spectrum when considering the full dataset over the whole studied time interval.

## 4 The shortest characteristic variability timescale of S5 1803+784

The light curve of the blazar S5 1803+784, obtained with high temporal resolution from TESS data (see Fig. 2), represents a superposition of variations occurring on multiple timescales. Assuming that at any given time moment the short-term variability is driven by a single dominant mechanism, either changing its parameters or being replaced by another one, it can be expected that the characteristic variability timescale

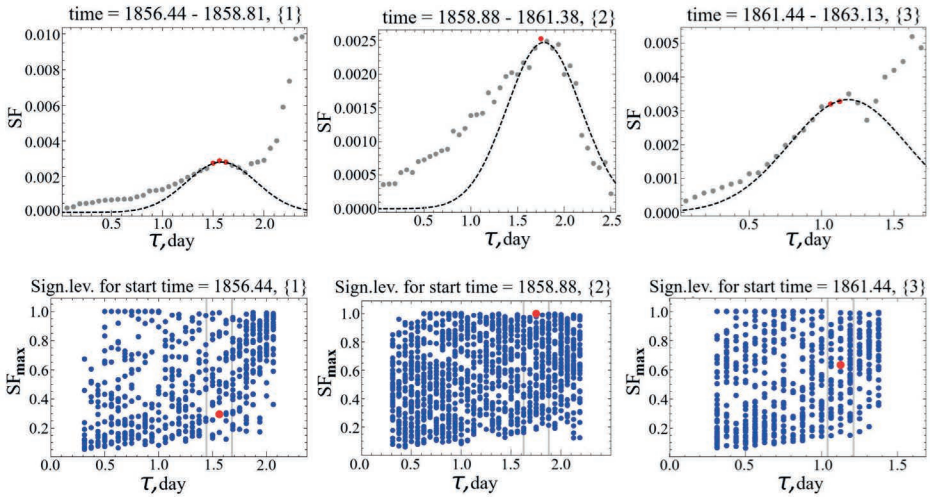



**Figure 4** Example of structure functions for consecutive intervals along the light curve (top panel) and the corresponding significance levels (bottom panel). Red dots indicate peaks of the SF plotted from observational data; blue dots correspond to peaks of the model light curves. Gray vertical lines mark the ±5% window within which the number $N$ of model SF maxima was counted.

$\tau$ will vary between different time intervals. One of the commonly used methods for estimating $\tau$ is the structure function (SF) (Simonetti et al. 1985). However, if the analysed time covers multiple changes in variability parameters, the different values of $\tau$ present in the data may obscure each other's signatures in the SF. Butuzova et al. (2025) proposed a method to identify the shortest variability timescale based on sequential addition of data points to a segment of the light curve until a maximum in the SF is detected. This maximum must exceed a predefined threshold to eliminate spurious peaks and must have a statistical significance of at least $p \geq 0.95$.

An example of selected segments on the light curve characterized by different $\tau$ values is shown in Fig. 4. The significance level was calculated as follows. The parameters of an ARIMA process, describing a given light curve segment, were estimated, and 1000 synthetic light curves were generated based on this process. For each synthetic light curve, the SF was computed, and its peak was searched for. These peaks were normalized to the maximum value of the corresponding SF. The significance level was calculated as $p = 1 - N/1000$, where $N$ is the number of synthetic SF peaks that (i) exceed the peak SF value from the observational data (normalized), and (ii) fall within a window of ±5% of the segment duration around the peak position of SF from the observational data (see Fig. 4, bottom panel).

The evolution of the mean magnitude, the characteristic variability timescale $\tau$, and the square of the average variability amplitude $\mathrm{SF}_{\mathrm{max}}$ (defined as the peak of the SF) is shown in Fig. 5. It is seen that $\tau$ can vary by a factor of several between adjacent time intervals, and there is no clear dependence on either the mean magnitude or $\mathrm{SF}_{\mathrm{max}}$ for the corresponding segment of the light curve.

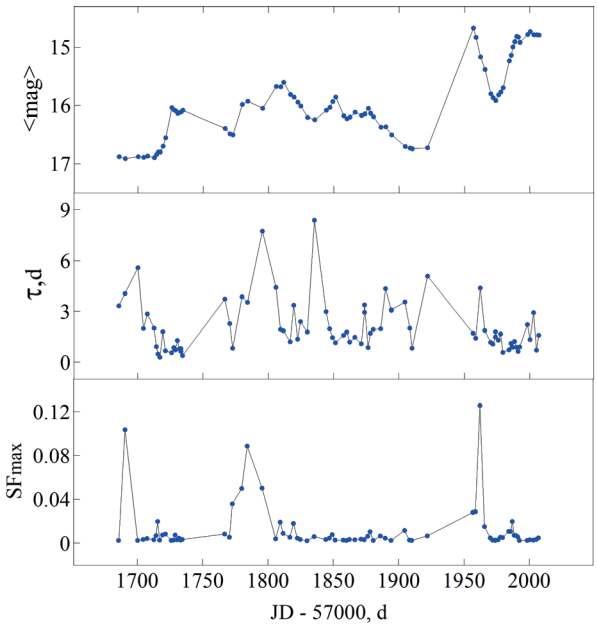



**Figure 5** Evolution of the mean magnitude, the characteristic variability timescale $\tau$, and the square of the average microvariability amplitude $SF_{max}$ (top to bottom).

## 5 Results and Conclusions

Figure 6 shows the correlations between microvariability parameters ($\tau$, $SF_{max}$, and $\langle mag \rangle$) and the spectral index. Visual analysis shows that significant changes in $SF_{max}$ for $\tau > 3$ coincide with positions near the peaks of flares, indicating rapid and significant brightness variations of the object during these periods.

Some apparent trends are observed in the bottom left plot of Fig. 6, suggesting a possible relation worth exploring. The square root of the structure function maximum,

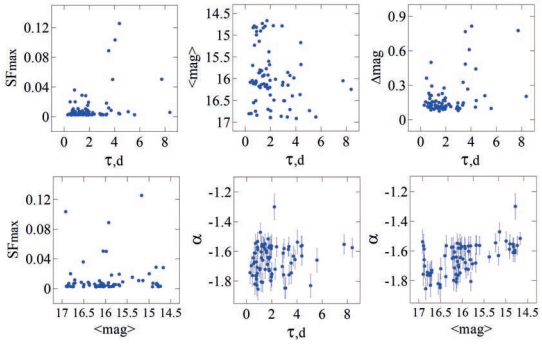



**Figure 6** Correlations between microvariability parameters ($\tau$, $SF_{max}$, and $\langle mag \rangle$) and the spectral index.

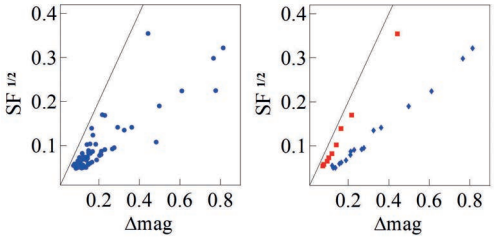



**Figure 7** Relation between the average amplitude of variability $SF_{max}^{1/2}$ and the maximum magnitude change $\Delta$mag for light curve segments with identified $\tau$. In the right plot, the points highlighted by red and blue colors correspond to two apparent linear dependencies. Their locations are indicated on the light curve (Fig. 8). The solid line indicates equality of the compared quantities.

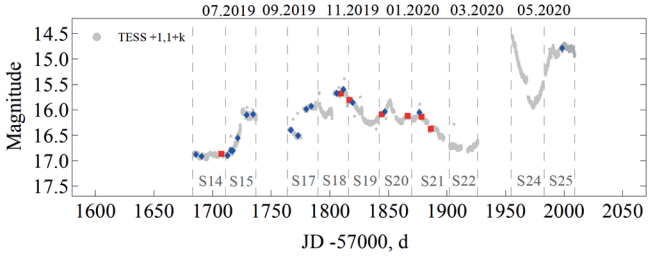



**Figure 8** Light curve of the blazar S5 1803+784 with highlighted segments corresponding to the linear correlations observed in Fig. 7.

$SF_{max}^{1/2}$, represents the average amplitude of variability within a given segment. The value $\Delta$mag denotes the maximum magnitude change in the same interval.

If these two parameters are approximately equal, then the overall brightness trend within the interval dominates in the short-term variability. If $SF_{max}^{1/2}$ is less than $\Delta$mag, then small fluctuations, superimposed on long-term trend, dominate in the variability on short-time scales. In the right panel of Fig. 7, we highlighted by red and blue colors the points corresponding to two apparent linear dependencies and indicate their locations on the light curve (Fig. 8).

The essence is as follows: if the highlighted points (e.g., red) are scattered across different parts of the light curve, the observed correlation is likely coincidental. Conversely, the blue points —particularly those within Sectors 15 and 17 — are closely clustered, suggesting the presence of a persistent physical process, which later either ceases or is masked by another process, possibly the same one with altered parameters.

Figure 9 visualizes the temporal and photometric variability properties. From the left panel of Fig. 9, no clear correlation is seen between the mean magnitude, the characteristic variability timescale $\tau$, and the spectral index $\alpha$, which is color-coded (green for flatter spectra, blue for steeper ones). However, a weak trend is evident: larger brightness tends to be associated with flatter spectra. The shortest variability timescales $\tau < 3$ days are observed across the full range of mean magnitudes and spectral indices, while values of $\tau > 3$ days tend to appear at intermediate $\alpha$.

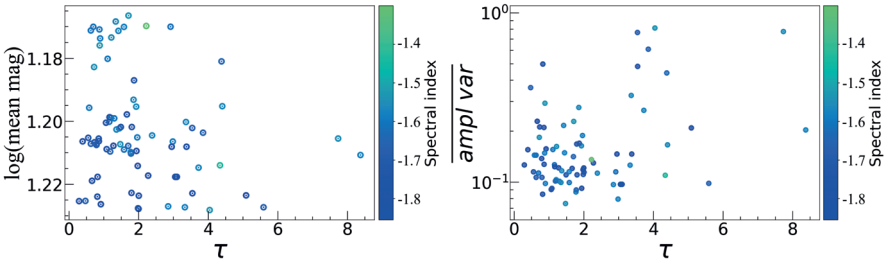



**Figure 9** Left panel: dependence between mean magnitude, characteristic variability timescale $\tau$, and spectral index (color-coded). Right panel: dependence between variability amplitude, characteristic variability timescale $\tau$, and spectral index (color-coded).

Naturally, the question arises as to whether selection effects may influence the results. We find that the selection effect is unlikely to have a significant influence on the results as the characteristic variability timescales are determined across the full range of the source's brightness. Regardless of the source's brightness state (faint, bright, or intermediate), the characteristic variability timescale may be either longer or shorter than three days. A similar pattern is seen in the spectral index: as noted above, it shows a weak tendency to increase with increasing blazar brightness and varies across the full magnitude range (from 17 to 15). Thus, $\tau$ was estimated for a range of both the spectral index and the source brightness. Therefore, the selection effect makes a minimal contribution to our conclusions. Nevertheless, the results may differ when data are analysed for a different time interval. We found no correlation between variability amplitude and $\tau$, in contrast to the interval from 24 July to 20 August 2021 (TESS Sector 41), which was previously analysed by Butuzova et al. (2025).

As our calculations have shown, $\tau$ does not depend on the source brightness or the spectral index. Based on these results, we suggest that the variability arises from the appearance and evolution of subcomponents within the jet, each characterized by different Doppler factors $\delta$ and volumes. The combination of these two parameters washes out any intrinsic correlations among the observed quantities. In our opinion, this is the simplest explanation for the observed behavior in terms of the so-called geometric effects (variations in the velocity of jet components and the viewing angle relative to the observer result in changes in the Doppler factor), as these effects are clearly present and have a significant influence. By subcomponent we refer to a portion of the jet flow that, due to inhomogeneities or instabilities, deviates from the main propagation axis. As a result, such a subcomponent possesses a Doppler factor different from that of the bulk jet. The superposition of many such subcomponents produces the observed day-scale variability. Butuzova (2021) has shown that the observed flattening of the optical spectrum with increasing brightness can be attributed to Doppler boosting of lower-frequency segments of the source-frame emission spectrum, which are intrinsically flatter due to natural causes. For example, the quadratic dependence of the rate of radiative energy losses on electron energy leads to a break in the electron energy spectrum. At energies below the break energy, the electron spectrum, and, consequently, the spectrum of synchrotron radiation produced by them, is flatter than at higher energies. On the other hand, due to synchrotron self-absorption, regions of the jet emitting at different frequencies and superimposed

to produce a power-law spectrum of blazar radiation are spatially separated, and the spectrum of an individual emission region becomes flatter and then inverted as the frequency decreases. The effect of synchrotron self-absorption in the optical range has been demonstrated in the jet of the blazar S5 0716+714 (Gorbachev et al. 2022). Thus, an increase in $\delta$ leads to an increase in observed flux, a shortening of the observed $\tau$, and a flattening of the spectral slope. These tendencies are seen in the left panel of Fig. 9, though strong correlations may be obscured by variation in the volumes of individual subcomponents. For example, two flares of similar amplitude may originate from (i) a large-volume, low-$\delta$ subcomponent or (ii) a small-volume, high-$\delta$ subcomponent. In the first case, no spectral change is observed; in the second case, significant spectral flattening may occur.

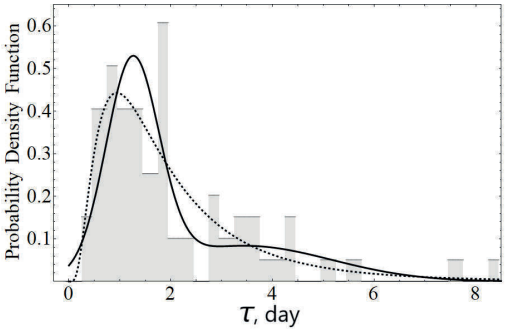



**Figure 10** Histogram of the distribution of characteristic variability timescales. Solid and dashed lines correspond to fitting with the mixture of two Gaussians and log-normal distribution, respectively. Two peaks are observed at 1.29 and 3.71 days.

The distribution of characteristic variability timescales is shown in Fig. 10. We approximated the distribution of $\tau$ using two models: a mixture of two Gaussians and a log-normal distribution (Fig. 10). The fitting parameters ($\chi^2$ and P-value) are given in Table 1. Although the $\tau$ distribution can formally be described by two Gaussian components, which could be interpreted as evidence of two distinct processes

**Table 1** Fitting parameters.

| Function | $\chi^2$ | P-Value |
|---|---|---|
| Mixture of two Gaussians | 19.9 | 0.0469 |
| Log-normal distribution | 8.65 | 0.655 |

operating in the jet, the log-normal distribution provides a better fit, as indicated by a lower $\chi^2$ and a higher P-value. This suggests that the observed distribution may arise from a single underlying process that produces a log-normal distribution of $\tau$. Since no correlation was found between $\alpha$, $\tau$, and magnitude, this supports the hypothesis of variability driven by evolving subcomponents with different physical properties.

***Main results***

1. Variability of the blazar S5 1803+784 during 07.2019 – 06.2020 occurred within a range of 2 magnitudes, and the spectral index varied between $-1.9$ and $-1.3$.
2. The absence of correlation between $\alpha$ and $\tau$ suggests that short-timescale variability is caused by subcomponents in the jet whose velocity vectors deviate from the main flow direction. Their distinct Doppler factors and evolution lead to the observed flux changes.
3. The distribution of $\tau$ corresponds to either the log-normal distribution indicating one short-term variability process or to the mixture of two Gaussian distributions resulting from the action of two processes of short-term variability.

## Acknowledgements

This work was supported by the Russian Science Foundation, No. 24-22-00343.

## References

Bellm E. C., Kulkarni S. R., Graham M. J. et al. (2019) PASP, 131, 018002
Bhatta G., Webb J. R., Hollingsworth H. et al. (2013) A&A, 558
Butuzova M. S. (2021) Astropart. Phys., 129, 102577
Butuzova M. S., Guseva V. A., Gorbachev M. A. et al. (2025) JHEAP, 45, 19
Gorbachev M. A., Butuzova M. S., Sergeev S. G., Nazarov S. V., Zhovtan A. V. (2022) ApJ, 928, 86
Gorbachev M. A., Butuzova M. S., Nazarov S. V., Zhovtan A. V. (2024) Astropart. Phys., 160
Hewitt A., Burbidge G. (1993) ApJS, 87, 451
Paiano S., Falomo R., Treves A., Scarpa R. (2020) MNRAS, 497, 94-108
Pushkarev A. B., Kovalev Y. Y., Lister M. L., Savolainen T. (2009) A&A, 507, L33-L36
Simonetti J. H., Cordes J. M., Heeschen D. S. (1985) ApJ, 296, 46